

An Actinide-boost Star Discovered in the Gaia-Sausage-Enceladus

Yangming Lin, Haining Li, Ruizheng Jiang, Wako Aoki, Satoshi Honda, Zhenyu He, Ruizhi Zhang, Zhuohan Li, Gang Zhao

<https://arxiv.org/abs/2505.07281>

Abstract

We report the discovery of an actinide-boost, very metal-poor ($[\text{Fe}/\text{H}] = -2.38$), r -process-enhanced ($[\text{Eu}/\text{Fe}] = 0.80$) star, LAMOST J0804+5740, within the Gaia-Sausage-Enceladus (GSE). Based on the high-resolution ($R \sim 36,000$ and $60,000$) and high signal-to-noise ratio spectra obtained with the High Dispersion Spectrograph on the Subaru Telescope, the abundances of 48 species are determined. Its $\log \epsilon(\text{Th}/\text{Eu}) = -0.22$ establishes it as the first confirmed actinide-boost star within the GSE. Comparative analysis of its abundance pattern with theoretical r -process models reveals that the magnetorotationally driven jet supernova r -process model with $\dot{L}_v = 0.2$ provides the best fit and successfully reproduces the actinide-boost signature. Kinematic analysis of actinide-boost stars reveals that approximately two-thirds of them are classified as ex situ stars, suggesting that actinide-boost stars are more likely to originate from accreted dwarf galaxies. As the first actinide-boost star identified within the GSE, J0804+5740 will provide valuable insights into r -process nucleosynthesis in accreted dwarf galaxies like the GSE, especially on the production of the heaviest elements.

Introduction

- Neutron-star mergers (NSM) are thought to be primary sites for r -process.
 - However, NSM scenarios face challenges in explaining the observed $[\text{Eu}/\text{Fe}]$ and $[\text{Fe}/\text{H}]$ relationship in very metal stars in the Milky Way due to their long merging timescales (C. Kobayashi 2023).
 - magneto-rotationally driven jet supernovae (MRDSN) and collapsar are also candidates for r -process site.
- Very-metal Poor (VMP) star ($[\text{Fe}/\text{H}] < -2.0$, which means $[\text{Fe}/\text{H}] < [\text{Fe}/\text{H}]_{\odot}/100$)
 - considered to be the oldest objects in the Universe.
 - preserves the chemical signatures at their formation
- possible to trace r -process events
- Gaia-Sausage-Enceladus (GSE) : substructure of Milky Way, which used to be the dwarf galaxy in the past
- “Actinide-boost” phenomenon
 - one-third of r -process-enhanced metal-poor stars exhibit $\log \epsilon(\text{Th}/\text{Eu})$ are roughly 0.4dex higher than those of other r -process-enhanced stars.
 - $\log \epsilon = \log[N(X)/N(H)] + 12$
 - The cause remains unidentified.
- J0804+5740 VMP star was identified to be the actinide-boost star.

Observations and Data analysis

- Subaru/HDS observation
 - spectra covering $4030\text{--}6800\text{\AA}$ with $R \sim 36000$ → elevated $[\text{Eu}/\text{Fe}]$ → identified as an r -II VMP star (pre-work)
 - spectra covering $3550\text{--}5210\text{\AA}$ with $R \sim 60000$ for further investigations (this work)
- T_{eff} and $\log g$ (surface gravity) are determined photometrically (H. Li et al. 2022).
 - They adopt color $(V - K_s) - T_{\text{eff}} - [\text{Fe}/\text{H}]$ relationship for T_{eff} from I. Ramírez & J.Meléndez (2005).
 - Parallax measurements from Gaia DR3
 - $\log g = \log g_{\odot} + \log \frac{M}{M_{\odot}} + 4 \log \frac{T_{\text{eff}}}{T_{\text{eff}\odot}} + 0.4 (M_{\text{bol}} - M_{\text{bol}\odot})$

Element Abundance

- Measure equivalent widths (EW) for over 600 lines and drive the abundances for 48 species.
 - derived by EW measurements or spectral synthesis (Figure 1).
 - adopt the 1D plane-parallel hydrostatic model atmosphere from the ATLAS NEWODF grid by F. Castelli & R. L. Kurucz (2003)

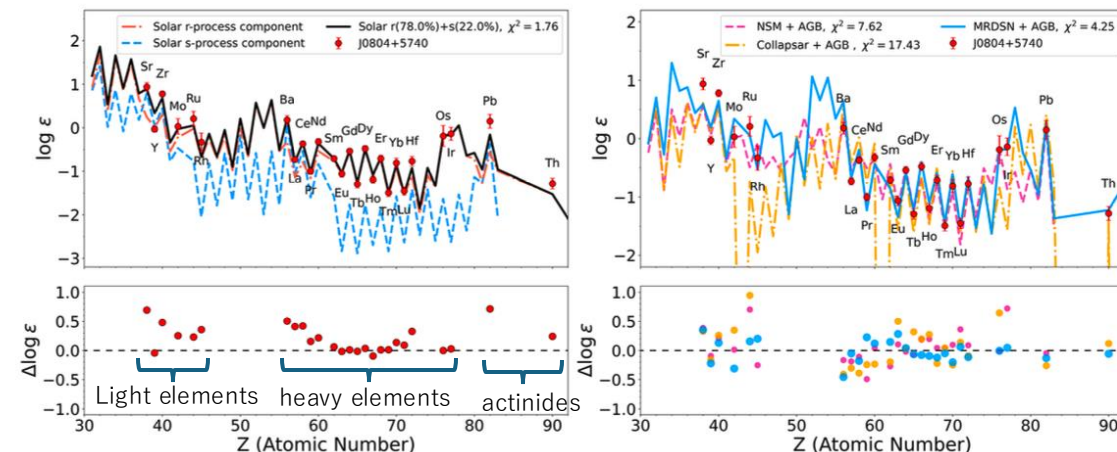


Figure 2. Top panel: the heavy-element abundance pattern for J0804+5740, compared with the solar r -process and s -process patterns (N. Prantzos et al. 2020; top left panel), as well as the theoretical r -process models combined with the asymptotic giant branch (AGB) s -process model (top right panel). The derived element abundances are depicted with red filled circles, with total error bars. Bottom panel: residuals between the derived element abundances and the solar r -process pattern (bottom left panel), as well as the theoretical r -process models combined with the AGB s -process model (bottom right panel) for J0804+5740.

Discussion

1. Abundance pattern

- The heavy elements abundance pattern accounts for 78% solar r -process + 22% s -process (Figure 2, left)
 - no significant radial velocity variation within 2σ → unlikely to be part of a binary system
 - No significant carbon enrichment ($[\text{C}/\text{Fe}] = 0.15$)
- J0804+5740 VMP star may not originate from a mass transfer event involving an asymptotic giant branch (AGB) companion star. Rather, the birth gas cloud of this star has been contaminated by the s -process
- Theoretical three models of NSM, MRDSN, and collapsar
 - MRDSN (r -process) + AGB (s -process) model** fits best for heavy and actinides elements abundance pattern (Figure 2, right).
 - Poor fits for light elements
- contributions from s -process, weak r -process and the light-element primary process are considered.

2. Kinematics

- employ deep-learning methodologies to distinguish between ex situ stars (originating from accreted dwarf galaxies) and in situ stars (formed within the Milky way) in the r -process enhanced metal-poor star with measurable Th sample (Z. Li et al. 2024) by Gaia DR3 data.
 - 6 ex situ stars and 3 in situ stars
 - Actinide-boost stars are more likely to originate from dwarf galaxies that were accreted by the Milky Way.

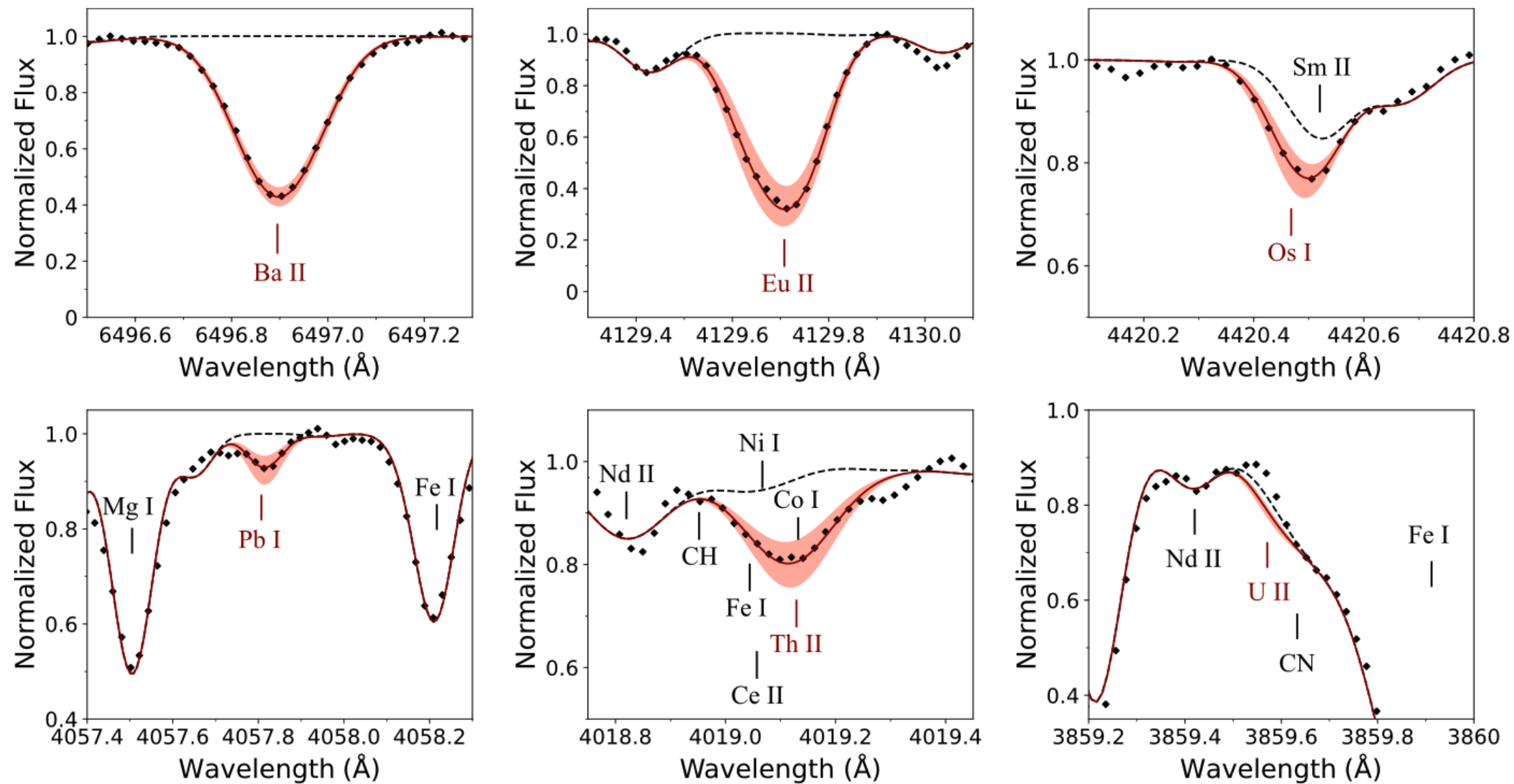


Figure 1. The spectral syntheses and the derived abundances for several key elements are presented. The black dots represent the observational spectrum. The red solid lines represent the best-fit syntheses, with an associated uncertainty of 0.2 dex (red shaded regions). The spectral syntheses excluding the elements of interest are shown as black dashed lines.

Table 1
Basic Parameters of J0804+5740

Parameter	Value	References
R.A. (hh:mm:ss)	08:04:52.8	Gaia Collaboration et al. (2023)
Decl. (deg:arcmin:arcsec)	57:40:19.4	Gaia Collaboration et al. (2023)
ℓ (deg)	159.86	Gaia Collaboration et al. (2023)
b (deg)	32.36	Gaia Collaboration et al. (2023)
V mag	11.510 ± 0.097	U. Munari et al. (2014)
K_s mag	8.859 ± 0.016	R. M. Cutri et al. (2003)
$E(B - V)$ (mag)	0.051 ± 0.011	G. M. Green et al. (2018)
RV_{helio} (km s^{-1})	-318.36 ± 0.15	This study
RV_{helio} (km s^{-1})	-318.08 ± 0.20	Gaia Collaboration et al. (2023)
RV_{helio} (km s^{-1})	-320.18 ± 3.15	A. L. Luo et al. (2022)
Parallax (mas)	0.284 ± 0.017	Gaia Collaboration et al. (2023)
Distance (kpc)	3.054 ± 0.181	F. Anders et al. (2022)
r_{apo} (kpc)	21.80 ± 0.12	This study
r_{peri} (kpc)	0.53 ± 0.20	This study
Z_{max} (kpc)	12.68 ± 2.65	This study
ecc	0.953 ± 0.018	This study
E ($10^3 \text{ km}^2 \text{ s}^{-2}$)	-131.74 ± 0.20	This study
J_r (kpc km s^{-1})	1555.22 ± 57.48	This study
J_ϕ (kpc km s^{-1})	226.39 ± 82.81	This study
J_z (kpc km s^{-1})	202.00 ± 19.86	This study
T_{eff} (K)	4585 ± 85	This study
T_{eff} (K)	4556 ± 93	H. Li et al. (2022)
$\log g$ (cgs)	1.41 ± 0.07	This study
$\log g$ (cgs)	1.45 ± 0.07	H. Li et al. (2022)
ξ (km s^{-1})	1.82 ± 0.02	This study
ξ (km s^{-1})	1.94 ± 0.05	H. Li et al. (2022)
[Fe/H]	-2.38 ± 0.09	This study
[Fe/H]	-2.47 ± 0.09	H. Li et al. (2022)

Table 2
Element Abundances of J0804+5740

Species	$\log \epsilon_\odot$	$\log \epsilon$	[X/H]	[X/Fe]	σ_{stat}	σ_{sys}	$\sigma_{\log \epsilon}$	$\sigma_{[\text{X}/\text{Fe}]}$	N	Method ^a
C (CH)	8.43	5.63	-2.80	-0.42	0.09	0.10	0.13	0.16	1	S
N (CN)	7.83	5.90	-1.93	0.45	0.09	0.18	0.20	0.22	1	S
O I	8.69	7.15	-1.54	0.84	0.09	0.06	0.11	0.14	1	S
Na I	6.24	4.08	-2.16	0.22	0.10	0.15	0.18	0.20	2	S
Mg I	7.60	5.57	-2.03	0.35	0.04	0.11	0.12	0.15	10	E
Al I	6.45	3.70	-2.75	-0.37	0.09	0.15	0.18	0.20	1	S
Si I	7.51	5.50	-2.01	0.37	0.06	0.12	0.14	0.16	2	E
Ca I	6.34	4.21	-2.13	0.25	0.02	0.08	0.08	0.12	32	E
Sc II	3.15	0.92	-2.23	0.15	0.03	0.03	0.04	0.10	15	S
Ti I	4.95	2.63	-2.32	0.06	0.02	0.14	0.14	0.17	29	E
Ti II	4.95	2.99	-1.96	0.42	0.02	0.03	0.04	0.10	40	E
V I	3.93	1.32	-2.61	-0.23	0.05	0.15	0.16	0.18	3	S
V II	3.93	1.63	-2.30	0.08	0.04	0.03	0.05	0.10	8	S
Cr I	5.64	2.89	-2.75	-0.37	0.02	0.14	0.14	0.17	14	E
Cr II	5.64	3.40	-2.24	0.14	0.05	0.03	0.06	0.11	5	E
Mn I	5.43	2.45	-2.98	-0.60	0.04	0.10	0.11	0.14	11	S
Fe I	7.50	5.05	-2.45	-0.07	0.01	0.12	0.12	0.15	128	E
Fe II	7.50	5.12	-2.38	0.00	0.02	0.02	0.09	0.13	18	E
Co I	4.99	2.40	-2.59	-0.21	0.04	0.16	0.17	0.19	9	S
Ni I	6.22	3.67	-2.55	-0.17	0.02	0.10	0.10	0.14	19	E
Cu I	4.19	1.08	-3.11	-0.73	0.09	0.13	0.16	0.18	1	S
Zn I	4.56	2.33	-2.23	0.15	0.06	0.02	0.07	0.11	2	E
Sr II	2.87	0.94	-1.93	0.45	0.06	0.07	0.10	0.13	2	S
Y II	2.21	-0.03	-2.24	0.14	0.03	0.06	0.07	0.11	14	E
Zr II	2.58	0.78	-1.80	0.58	0.03	0.05	0.06	0.11	21	E
Nb II	1.46	<-0.01	<-1.47	<0.91	1	S
Mo I	1.88	0.03	-1.85	0.53	0.09	0.16	0.18	0.21	1	S
Ru I	1.75	0.21	-1.54	0.84	0.06	0.16	0.17	0.19	4	S
Rh I	0.91	-0.33	-1.24	1.14	0.12	0.17	0.21	0.23	2	S
Ba II	2.18	0.18	-2.00	0.38	0.06	0.07	0.10	0.13	5	S
La II	1.10	-0.73	-1.83	0.55	0.01	0.06	0.06	0.11	18	S
Ce II	1.58	-0.37	-1.95	0.43	0.02	0.06	0.06	0.11	39	E
Pr II	0.72	-1.00	-1.72	0.66	0.02	0.07	0.07	0.11	6	S
Nd II	1.42	-0.32	-1.74	0.64	0.02	0.07	0.07	0.12	50	E
Sm II	0.96	-0.71	-1.67	0.71	0.02	0.05	0.06	0.11	31	E
Eu II	0.52	-1.06	-1.58	0.80	0.02	0.07	0.08	0.12	5	S
Gd II	1.07	-0.54	-1.61	0.77	0.04	0.05	0.06	0.11	16	E
Tb II	0.30	-1.29	-1.59	0.79	0.06	0.07	0.09	0.13	2	E
Dy II	1.10	-0.48	-1.58	0.80	0.04	0.05	0.07	0.11	13	E
Ho II	0.48	-1.19	-1.67	0.71	0.05	0.06	0.08	0.12	3	S
Er II	0.92	-0.71	-1.63	0.75	0.04	0.06	0.08	0.12	8	E
Tm II	0.10	-1.49	-1.59	0.79	0.08	0.05	0.09	0.13	3	E
Yb II	0.84	-0.81	-1.65	0.73	0.09	0.06	0.11	0.14	1	S
Lu II	0.10	-1.45	-1.55	0.83	0.09	0.03	0.09	0.13	1	S
Hf II	0.85	-0.77	-1.62	0.76	0.09	0.05	0.11	0.14	1	S
Os I	1.40	-0.19	-1.59	0.79	0.17	0.17	0.24	0.26	2	S
Ir I	1.38	-0.14	-1.52	0.86	0.09	0.12	0.15	0.18	1	S
Pb I	1.75	0.15	-1.60	0.78	0.09	0.13	0.16	0.18	1	S
Th II	0.02	-1.28	-1.30	1.08	0.09	0.08	0.12	0.15	1	S
U II	-0.54	<-1.87	<-1.33	<1.05	1	S

Note.

^a The method used to derive the abundance is indicated as follows: "E" denotes that the abundance is derived from EWs, while "S" signifies that the abundance is derived from spectral synthesis.

C-enrichment model by mass transfer from AGB star

恒星の化学組成にもとづく研究例②

連星系の相互作用— 炭素や重元素(s-process元素)の増大

